ADVANCED BIOLOGY
www.advanced-bio.com

Temporal Dynamics of Metabolic Acquisition in Grafted Engineered Human Liver Tissue

*Chelsea L. Fortin, Tara N. McCray, Sarah H. Saxton, Fredrik Johansson, Christian B. Andino, Jonathan Mene, Yuliang Wang, and Kelly R. Stevens**

Liver disease affects millions globally, and end-stage liver failure is only cured by organ transplant. Unfortunately, there is a growing shortage of donor organs as well as inequitable access to transplants across populations. Engineered liver tissue grafts that supplement or replace native organ function can address this challenge. While engineered liver tissues have been successfully engrafted previously, the extent to which these tissues express human liver metabolic genes and proteins remains unknown. Here, it is built engineered human liver tissues and characterized their engraftment, expansion, and metabolic phenotype at sequential stages post-implantation by RNA sequencing, histology, and host serology. Expression of metabolic genes is observed at weeks 1–2, followed by the cellular organization into hepatic cords by weeks 4–9.5. Furthermore, grafted engineered tissues exhibited progressive spatially restricted expression of critical functional proteins known to be zonated in the native human liver. This is the first report of engineered human liver tissue zonation after implantation in vivo, which can have important translational implications for this field.

1. Introduction

The liver is the largest internal organ and performs hundreds of essential functions for human health. Liver disease is a significant global health burden, causing over 40,000 annual deaths in the United States alone and more than one million worldwide deaths each year.[1] While liver transplant is curative, less than ten thousand occur per year in the US.[2] There is also a growing shortage of donor organs and disparities in equitable access to transplants amongst non-white, women, uninsured, and rural populations.[3] Less than 10% of global transplantation needs are currently met,[4] highlighting the demand for alternative therapies. Engineered liver tissue that supplements organ function could bridge patients to transplant and help alleviate the donor tissue shortage.[5] To reach the clinic, engineered liver tissues would ideally mimic key structural and physiological aspects of the native liver.

The hundreds of functions performed by the native liver can be broadly categorized into axes such as protein synthesis, amino acid metabolism, nitrogen clearance, bile handling, drug detoxification, lipid and cholesterol homeostasis, glycogen storage, and more.[6] To achieve all these tasks, the liver "divides and conquers" by delegating roles into distinct regions or "zones" across each functional unit of the liver, called lobules. Each liver lobule lies between two blood circulatory hubs, the portal triad (consisting of the portal vein, biliary duct, and hepatic artery) and the central vein.[7] The zone near the portal triad is rich in oxygen and can support metabolic activities like gluconeogenesis and urea synthesis, while the zone around the central vein is oxygen-poor and resorts to glycolysis and is the site of drug detoxification. The term "zonation" refers to this separation of activity into distinct spatial regions. For implanted tissue to be broadly applicable in the clinic and perform a spectrum of the functions typically performed by the native liver, engineered tissues must replicate this zonal morphology and function.

While a variety of models to study liver disease in vitro have sought to replicate liver zonation, such as liver slices and microfabricated organ-on-chip platforms,[8] mimicking zonal phenotypes in implanted tissue in vivo has not been explored. We and others have previously developed engineered

C. L. Fortin, T. N. McCray, S. H. Saxton, F. Johansson, C. B. Andino, J. Mene, Y. Wang, K. R. Stevens
Institute for Stem Cell & Regenerative Medicine
University of Washington
Seattle, Washington 98109, USA
E-mail: ksteve@uw.edu

C. L. Fortin, T. N. McCray, S. H. Saxton, F. Johansson, C. B. Andino, J. Mene, K. R. Stevens
Department of Bioengineering
University of Washington
Seattle, Washington 98105, USA

C. L. Fortin, K. R. Stevens
Department of Laboratory Medicine and Pathology
University of Washington
Seattle, Washington 98195, USA

Y. Wang
Department of Computer Science & Engineering
University of Washington
Seattle, Washington 98195, USA

The ORCID identification number(s) for the author(s) of this article can be found under https://doi.org/10.1002/adbi.202200208.

DOI: 10.1002/adbi.202200208

implantable human liver tissue grafts with the future goal of studying and supplementing liver function.[9] In one formulation, engineered tissues are composed of liver primary human hepatocytes (HuHep), normal human dermal fibroblasts (NHDF), and human umbilical vein endothelial cells (HUVEC) encased within fibrin hydrogel. This tissue not only carries out critical human liver functions and transcriptionally resembles the human liver, but also expands in response to the mouse hosts' chronic, progressive liver injury.[9] However, early studies focused on building the human liver tissue and thus only examined explanted tissues at a single time point (12 weeks) after implantation and characterized the expression of only a few hepatic functional proteins. The extent to which such tissues express a larger subset of hepatic functional markers and importantly also replicate the spatial zonal phenotype of the native liver remains unknown. To bring engineered tissues closer to the clinic, a more comprehensive characterization of morphology and metabolic phenotype is needed.

Here, the dynamics of metabolic phenotype within engineered human liver tissues were studied after implanting into mice with chronic and progressive liver injury. To evaluate metabolic maturity, a time-course characterization of both RNA expression and protein localization within human liver grafts after implantation was performed. This work identifies phenotypes within the engineered tissues that resemble the zonation found in the native human liver. Metabolic zonation is a necessary component of liver function and is indispensable for successfully engineered tissues to reach the clinic. To our knowledge, this is the first report of bioartificial human hepatic zonation in vivo.

2. Results and Discussion

2.1. Time Course Characterization of Engineered Human Liver Tissue Graft Expansion

We first sought to rigorously characterize the expansion dynamics of engineered implantable liver tissue created from HuHep, NHDF, and HUVEC within fibrin hydrogel (**Figure 1**A).[9] HuHep were aggregated with NHDF using aggrewells before suspension in fibrin hydrogel with HUVEC. Grafts were implanted ectopically into the gonadal fat pad of fumarylacetoacetate hydrolase, recombination activating gene 2, and interleukin-2 receptor subunit gamma null on non-obese diabetic background (FRGN) mice. This mouse model experiences progressive liver injury unless treated with nitisinone (NTBC).[10] NTBC was therefore cycled on and off to trigger chronic host liver injury and regeneration, along with concomitant stimulation of ectopic human liver graft growth. After implantation, grafts were characterized at five sequential time points during expansion from week 1 to week 9.5 by RNA sequencing, histology, and host serology (Figure 1A, Figure S1A, Supporting Information).

To interrogate graft morphology over time post-implant, tissues were collected for immunostaining and histology (Figure 1B–F). Throughout the course of engraftment, engineered liver tissue self-organized to resemble the native human liver in epithelial structure (Figure 1B); 4.5 weeks after implantation, hepatocytes were densely packed and typically appeared as large cells with a low cytoplasmic to nuclear ratio.[11] Some binucleated cells were observed (Figure 1B, inset, asterisk). By weeks 7–9.5, engineered tissues were arranged into cord-like structures of cells encased by a collagen-rich matrix that resembled the native morphology of the human liver (Figure 1C). Grafted cells expressed markers associated with hepatocytes, such as CK18 and the functional protein albumin (ALB), and these became more prominently expressed after 2 weeks of engraftment (Figure 1D,F). Rare, CK19-positive cells, a marker of biliary epithelial cells and hepatic progenitor cells, were also observed (Figure 1E).

Quantification of the human hepatocyte area within the grafts (CK18+ area, red line, Figure 1G) demonstrated an increase in graft size over time. Quantification of EdU incorporation revealed that there was an initial burst of hepatocytes undergoing DNA replication between weeks 1 and 2 after implant, followed by a drop-off in DNA replication as grafts continue to expand, possibly by cellular hypertrophy.[12] Notably, hepatocyte cytoplasm appeared eosinophobic (likely protein-sparse) during the DNA replication phase at weeks 1–2, with cytoplasmic content recovering and appearing more eosinophilic (protein-dense) by week 4.5 (Figure 1B,C).

To monitor liver function, host blood was collected for serological assessment of human liver proteins by ELISA (Figure 1G). The secreted liver protein ALB was detected at each time point and its concentration in host blood increased over time, indicating increased liver function accompanying graft expansion. The most rapid rise in ALB production occurred between 1- and 2-weeks postengraftment, followed by sustained protein expression.

2.2. Engineered Human Liver Tissue Shows Increased Metabolic Capacity Over Time

To investigate the transcriptome of engineered liver tissues during expansion, bulk RNA was collected for RNA sequencing (RNAseq) in triplicate at weeks 1–9.5 after implant (Figure S1A,B, Supporting Information). The number of reads in the bulk RNA samples showed increasing content mapping to the human genome over time (Figure S1C, Supporting Information), indicating that samples became more enriched in human gene expression with graft growth, with fewer transcripts mapping to the murine hosts' genome. We then sought to further characterize the expression of genes associated with liver-specific functions throughout graft development. To do this, the expression of genes belonging to a hepatic signature in the engineered livers was visualized by a heatmap (**Figure 2**A). Most samples from later time points (10 out of 12 samples) after engraftment clustered together and separated from week 1, indicating a different transcriptional landscape after grafts are established in vivo. Two samples, one from week 4.5 and one from week 9.5, regularly clustered with the week 1 samples due to the high expression of fibrinogen beta, alpha, and gamma chain genes (*FGB*, *FGA*, *FGG*) and serum amyloid A1 and -2 genes (*SAA1*, *SAA2*) which were also highly expressed at week 1 (Figure 2A, Figure S1B, Supporting Information).

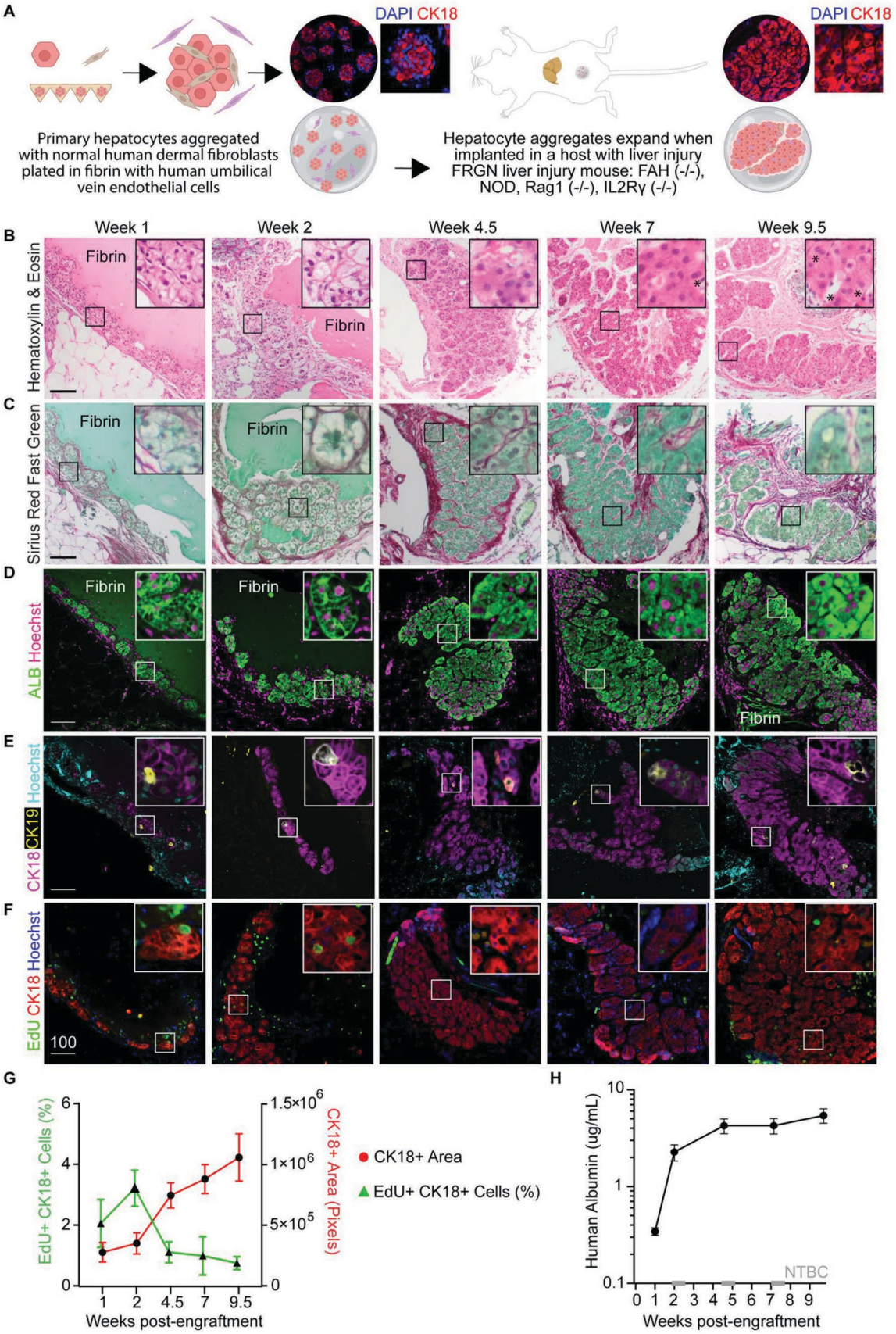

We observed that genes commonly associated with liver regeneration such as hepatocyte growth factor (*HGF*) and cyclin D1 (*CCND1*) were expressed early after implantation, along with ADP-ribosylation factor 6 (*ARF6*) and GATA-binding protein 6 (*GATA6*) which are important in hepatogenesis (Figure 2A).[13,14] Notably, the course of early expression of such genes associated with liver regeneration largely matched the course of Ki67 protein expression by hepatocytes, further supporting the notion that at least some graft expansion was driven by early hepatocyte replication (Figure 1G).

Importantly, we further noted that a multitude of genes responsible for diverse hepatic functions such as mercaptopyruvate sulfurtransferase (*MPST*), *ALB*, *ASS1*, glutathione S-transferase alpha 2 (*GSTA2*), asialoglycoprotein receptor 1 (*ASGR1*), carbamoyl-phosphate synthase 1 (*CPS1*), transthyretin (*TTR*), and multiple cytochrome p450 genes showed increased expression over time after tissue implantation. This high metabolic gene signature was also observed by gene set enrichment analysis using iPathwayGuide (Figure S2, Supporting Information). Thus, sequencing data suggested that genes associated with metabolic activities become upregulated with increased engraftment time in vivo.

To further characterize the metabolic maturation of grafted engineered liver tissues over time after implantation, we next immunostained graft sections for various functional proteins that represent key "axes", or categories, of liver functions beyond protein production (Figure 1D,H), including xenobiotic metabolism, amino acid metabolism, and mitochondrial content (Figure 2B–F).[15] One of the metabolic functional axes of the liver is amino acid metabolism and subsequent clearance of excess ammonia in the form of urea via the ornithine (urea) cycle. ASS1 (Figure 2B, red) is an enzyme that functions in the third step of this process to combine the amino acids citrulline and aspartate to form argininosuccinic acid, a precursor to arginine.[16] Arginine is then hydrolyzed during the final step by ARG1 (Figure 2C, pink) to form urea, for ammonia detoxification, and to form ornithine which is used for cell proliferation and collagen formation.[17] Both ASS1 and ARG1 were expressed by engineered liver tissues and detectable throughout all growth stages.

Second, we sought to query the presence of proteins associated with xenobiotic (e.g., drugs and alcohol) detoxification, which is partly carried out by sequential cytochrome p450 enzyme processes. First, we interrogated CYP2A6, a cytochrome p450 enzyme involved in the metabolism of ≈3% of drugs.[18] Expression of CYP2A6 was not detected at weeks 1 and 2 but was observed at week 4.5 onward (Figure 2D, green). This is notable because modeling human CYP2A6 in vivo has remained challenging, as rodents exhibit species-specific variability in CYP2A6 activity.[19] CYP2E1, a cytochrome p450 enzyme that catalyzes the oxidation of endobiotics, such as retinoids, is commonly studied in alcohol detoxification. Like CYP2A6 expression, we found that CYP2E1 protein expression was low at week 1 and became more prominent over time after engraftment (Figure 2E, cyan). However, CYP2E1 was detected at week 2 while CYP2A6 was not.

Finally, mitochondria are key metabolic hubs for hepatocyte homeostasis, flexibility, and survival.[15] Some cytochrome p450 enzymes are also localized in the mitochondria.[20] We found that the amount of mitochondrial content increased within human engineered liver tissue with increasing time of engraftment (Figure 2F, brown), like observations for CYP2E1 and CYP2A6.

Collectively, these data indicate RNA and protein expression of genes associated with hepatocyte identity and function arise in engineered human livers between weeks 1 and 2, followed by increased expression of several key metabolic functional proteins with increasing time following engraftment.

2.3. Engineered Human Liver Tissues Show a Zonated Phenotype

When exploring the expression of metabolic proteins within engineered liver grafts, we observed that some proteins, such as CYP2A6 and CYP2E1, appeared to be expressed heterogeneously across the hepatic graft (Figure 2D,E). We were intrigued by this, as in the native liver many functional genes and proteins are often "zonated", such that their expression varies spatially across the liver lobule (**Figure 3**A). Thus, we next further characterized if engineered transplantable human liver grafts recapitulate aspects of metabolic zonation of native human liver. First, we further examined the expression of genes belonging to metabolic pathways that have zonated activity (Figure 3B), with genes that exhibit zonated protein expression marked in red in Figure 3B. We found that a majority of zonated human liver genes were expressed by week 2 postimplant by engineered human liver tissues.

Figure 1. Time course characterization of engineered human liver tissue grafts. A) Diagram depicting the construction of engineered human liver tissue grafts: HuHep are aggregated with NHDF and then polymerized within fibrin with HUVEC. Grafts are implanted ectopically into mice with liver injury (FRGN mice). B) Hematoxylin and eosin staining of engineered liver tissue grafts explanted at weeks 1–9.5. Nuclear content was stained with hematoxylin and basic compounds (proteins) were stained with eosin (right). Asterisk indicates binucleate cells. C) Sirius red and fast green staining of engineered liver tissue grafts from weeks 1–9.5. Collagen was stained with Sirius red, and protein was counterstained with fast green (middle, right). D) Immunostaining for hepatocyte marker albumin (ALB, green) and DNA (Hoechst, magenta) in engineered liver tissue grafts from weeks 1–9.5. E) Immunostaining for hepatocyte marker cytokeratin 18 (CK18, pink), biliary epithelial marker cytokeratin 19 (CK19, yellow), and DNA (Hoechst, blue) in engineered liver tissue grafts from weeks 1–9.5. F) Immunostaining for hepatocyte marker CK18 (red), 5-ethynyl-2′-deoxyuridine (EdU) incorporation (green), and DNA (Hoechst, blue) in engineered liver tissue grafts grown from weeks 1–9.5. In Figure 1B–F, ≥3 grafts from separate mouse hosts were stained for each panel at each time point; one representative graft is shown. Scale bars display 100 μm. G) The percentage of cells undergoing DNA replication, EdU+ nuclei (green, triangle), in the CK18+ area (red, circle), as quantified from the immunostaining performed in Figure 1F. Error bars represent the standard error of the mean. H) Results from an enzyme-linked immunosorbent assay (ELISA) for human albumin (μg mL^{-1}) from the blood of mice implanted with human liver grafts. Serum was collected at weeks 1, 2, 4.5, 7, and 9.5. NTBC was pulsed three times during graft growth and is shown in gray along the *x*-axis. Data is presented as mean +/- standard error of the mean. Sample size is three mice per timepoint.

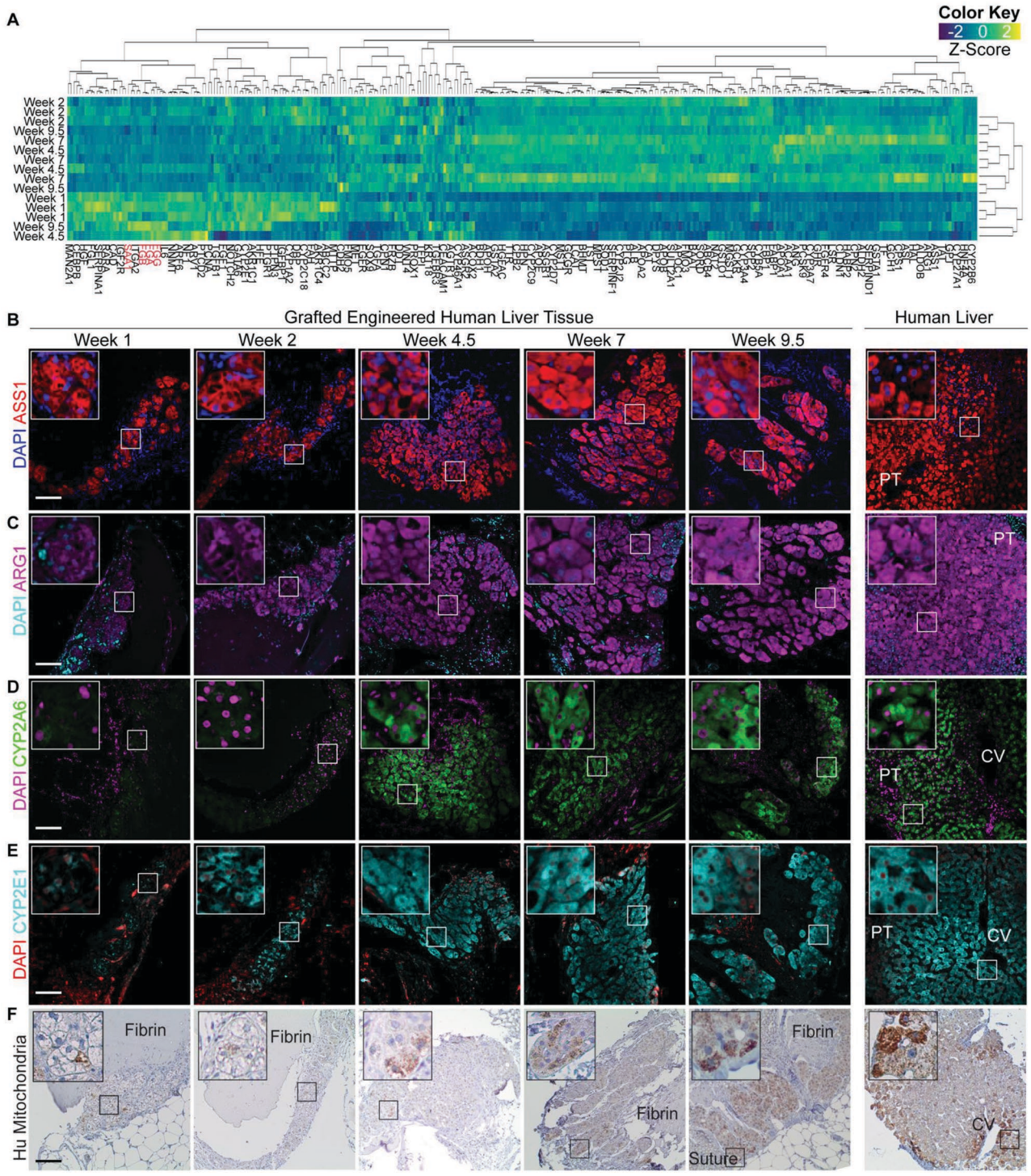

Figure 2. Engineered human liver tissue shows increased metabolic capacity over time. A) Heatmap of liver-specific gene expression. Bulk RNA was collected and sequenced in triplicate from implanted grafts grown to weeks 1, 2, 4.5, 7, and 9.5 in separate mice. A heatmap plot was generated from transcripts per million of 276 genes from the liver gene set enrichment lists SU_LIVER (M7054) and HSIAO_LIVER_SPECIFIC_GENES (M13283).[21,22] Corresponding *Z*-scores are shown for each row of genes. Hierarchical clustering was performed by Pearson correlation on rows and by Spearman for columns. Some genes that are driving the clustering of week 4.5 and week 9.5 with week 1 samples are highlighted in red. B) Immunostaining for argininosuccinate synthase (ASS1,red) and DNA (DAPI, blue) in engineered liver tissue grafts from weeks 1–9.5. C) Immunostaining for arginase 1 (ARG1, pink) and DNA (DAPI, cyan) in engineered liver tissue grafts from weeks 1–9.5. D) Immunostaining for cytochrome P450 family 2 subfamily A member 6 (CYP2A6, green) and DNA (DAPI, pink) in engineered liver tissue grafts from weeks 1–9.5. E) Immunostaining for cytochrome P450 family 2 subfamily E member 1 (CYP2E1, cyan) and DNA (DAPI, red) in engineered liver tissue grafts from weeks 1–9.5. F) Immunostaining for human (Hu) mitochondria (brown) and DNA (hematoxylin, blue) in engineered liver tissue grafts from weeks 1–9.5. In Figure 2B–F, ≥3 grafts from separate mouse hosts were stained for each panel at each time point; one representative graft is shown. Scale bars display 100 μm. CV = central vein, PT = portal triad.

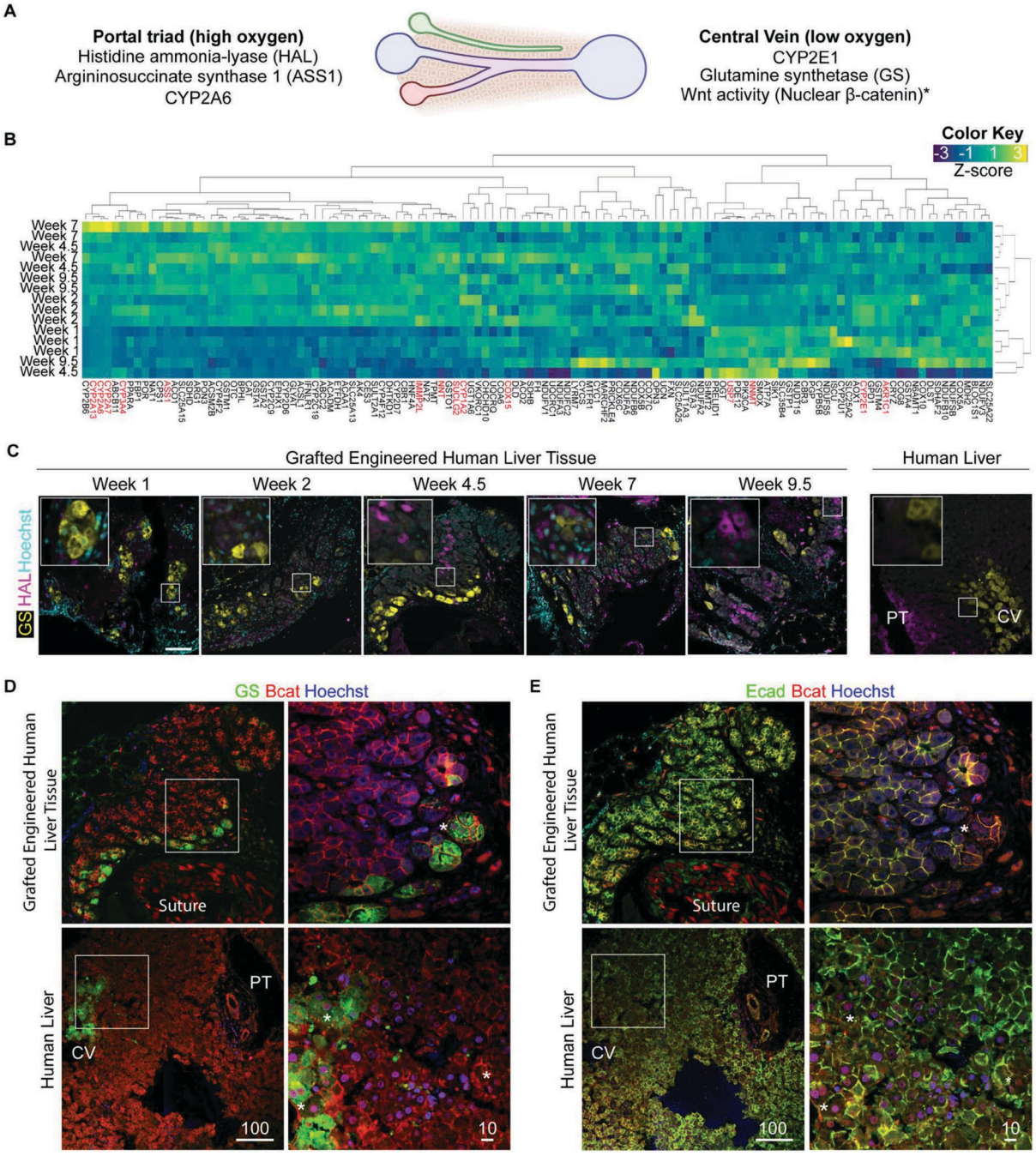

Figure 3. Engineered human liver tissues show a zonated phenotype. A) Diagram of the liver lobule with corresponding zonated protein expression found at the portal triad or central vein. * = Reported in rodents.[22–24] B) Heatmap of metabolic genes from zones 1, 2, and 3 of the liver. Bulk RNA was collected and sequenced in triplicate from implanted grafts grown to weeks 1, 2, 4.5, 7, and 9.5. A heatmap plot was generated from transcripts per million of genes related to liver metabolism. Corresponding *Z*-scores are shown for each row of genes. Hierarchical clustering was performed by Pearson correlation on rows and by Spearman for columns. The gene list was curated from the Gene Ontology (GO) terms: xenobiotic metabolic process, catabolic process, steroid metabolic process, glycoprotein metabolic process, lipoprotein metabolic process, carbohydrate metabolic process, cholesterol metabolic process, cellular respiration (oxidative metabolic process, oxidative metabolism, respiration), regulation of gluconeogenesis, urea metabolic process, glutamine synthesis, positive regulation of lipid biosynthetic process. Terms were chosen based on pathways that are functional at the portal triad and central vein of the liver lobule. Gene names highlighted in red appear zonated on the Human Protein Atlas (proteinatlas.org). C) Immunostaining for glutamine synthetase (GS, yellow), histidase (HA, pink), and DNA (Hoechst, cyan) in engineered liver tissue grafts from weeks 1–9.5. D) Immunostaining for GS (green), β-catenin (red), and DNA (Hoechst, blue) in engineered liver tissue grafts grown for 4.5 weeks (top) and native human liver (bottom). Asterisk indicates nuclear localization. Inset scale bars display 10 µm. E) Immunostaining for E-cadherin (Ecad, green), β-catenin (red), and DNA (Hoechst, blue) in engineered liver tissue grafts grown for 4.5 weeks (top) and native human liver (bottom). Asterisk indicates nuclear localization. Inset scale bars display 10 µm. In Figure 3C–E, ≥3 grafts from separate mouse hosts were stained for each panel at each time point; one representative graft is shown. Scale bars display 100 µm. CV = central vein, PT = portal triad.

To validate these findings, we next explored proteins that exhibit strict demarcation in their zonated expression in the human liver. First, we immunostained implanted engineered tissue grafts for HAL (Figure 3C, pink), which is responsible for the catabolism of histidine to transurocanic acid and ammonia and is expressed around the portal triad in the human liver. We found that HAL was restricted to the graft:host interface in engineered livers (Figure 3C). GS (Figure 3C, yellow) is important in nitrogen metabolism to synthesize glutamine from glutamate and ammonia. In the human liver, GS has only expressed in the first 1–3 cell layers surrounding the central vein. This was also consistent in grafts where only the first few cells inward from the graft periphery were positive for GS.

In rodents, β-catenin is required for zonation and expression of GS, and its inhibition results in a periportal phenotype.[23–25] The expression and localization of β-catenin were assessed by immunostaining in both human liver and engineered liver tissue (Figure 3D). In the absence of the wingless-related integration site (Wnt) ligand, β-catenin will either be sequestered at the membrane and associated with Ecad or in the cytoplasm marked for degradation by the destruction complex.[26] In the presence of Wnt, β-catenin will become stabilized and enter the nucleus to induce the expression of Wnt genes, such as *GS*. In human liver tissue, nuclear β-catenin was observed at and around the central vein, as well as throughout the liver lobule (Figure 3D, upper). In engineered human liver tissue, nuclear β-catenin was difficult to observe but was detectable in regions that were co-expressing GS (Figure 3D, lower, asterisk). When β-catenin was not observed in the nucleus it was localized at the membrane near Ecad (Figure 3E).

Finally, we sought to characterize the spatial expression of a protein that is zonated differently between species, in this case, humans versus mice. We immunostained for Ecad protein, which is zonated in mice but not in the human liver.[27] We found that like human liver tissue, Ecad was expressed uniformly (i.e., not zonated) across engrafted engineered liver tissues. Thus, engineered human liver tissue could serve as an important model system that recapitulates various aspects of human metabolic zonation.

2.4. Human Nonparenchymal Cells are not Required for the Zonated Phenotype in Engineered Liver Tissue

Rodent liver zonation is directed by oxygen gradients, Wnt molecules, and other signals originating in part from nonparenchymal cells (NPC) in the native liver, such as central vein endothelial cells.[28] We thus wondered the extent to which expression of metabolic markers and zonation of engineered human liver tissues was dependent upon the inclusion of the HUVEC and NHDF in the engineered tissue. We set out to further characterize implanted engineered liver tissue grafts fabricated with and without NPC (NHDF or HUVEC, **Figure 4**A).

We fabricated engineered liver tissues with and without NPC and engrafted these tissues into FRGN mice. As our earlier data showed robust graft formation within the mice by two weeks, we chose this timepoint to further investigate NPC contributions to graft metabolism. After two weeks of engraftment, both engineered liver tissues consisting of HuHep alone and HuHep with NPC expressed proteins that are important for metabolic function and zonation, such as cCYP3A (Figure 4B), CYP2E1 (Figure 4C), ALB (Figure 4D), ASS1 (Figure 4E) and GS (Figure 4E). CD31, expressed by endothelial cells, was observed in grafts with and without NPC (Figure 4C). In the grafts that were generated without HUVEC NPC, the CD31-positive cells are most likely of host origin, and it has been previously reported that host circulation connects to grafts after implant and ultimately becomes chimeric.[9] Notably, GS expression was detected at the graft periphery in a zonated pattern in both graft formulations. This suggests that, while supportive factors from HUVEC or NHDF are important to promote graft expansion,[9] they are not required to induce the expression of zonated proteins by human hepatocytes in engineered human livers. We noted that in both tissues with and without NPC, GS tended to be localized to the graft border, near the interface between the graft and host tissues. The drivers of the zonated phenotype may be originating from the adjacent host tissue or the host circulation.

3. Conclusion

The present study used RNAseq, immunostaining, and host serology to characterize the molecular landscape and metabolic maturation of engineered human liver tissue expansion. After implanting in mice experiencing liver injury, engineered liver grafts expressed genes and proteins that are important in liver metabolic function. In the native liver, many metabolic functions are spatially delegated to different populations of hepatocytes depending on their proximity to the major blood vessels, a phenomenon termed "liver zonation." The expression of proteins that are zonated in the native liver also appeared to be zonated in the engineered liver. This report not only brings these engineered tissues closer to relevance for the clinic but also offers the field a platform to study the mediators that establish human liver zonation.

Observations mirrored aspects of rodent liver regeneration, where hepatocyte metabolic activity is reduced in the early stages of liver regeneration and increases steadily over time thereafter.[29] Rodent livers that are expanding after surgical resection show a reduction in glycogen content, serum glucose, and metabolic pathway gene expression,[29] with a switch to oxidation to produce metabolites and energy.[30] The metabolic stress transitions cells from quiescence to proliferation[31] which corresponds with the downregulation of amino acid biosynthesis.[29] This is reminiscent of the eosinophobic cytoplasm observed during DNA replication at weeks 1 and 2 of engineered graft expansion and the lack of CYP2E1 and CYP2A6 at early time points after engineered liver tissue engraftment. Data suggest that either xenobiotic metabolism was not required until week 4.5 after engraftment, or the engineered livers did not have the capacity for xenobiotic metabolism until cell division had lessened. These results agree with rodent models of liver regeneration where cytochrome p450 enzyme expression is reduced while cells are dividing.[32–34] Similarly, mitochondria are an important component of metabolic function, but mitochondrial content was very low at early time points during cell division when organelles are disrupted.

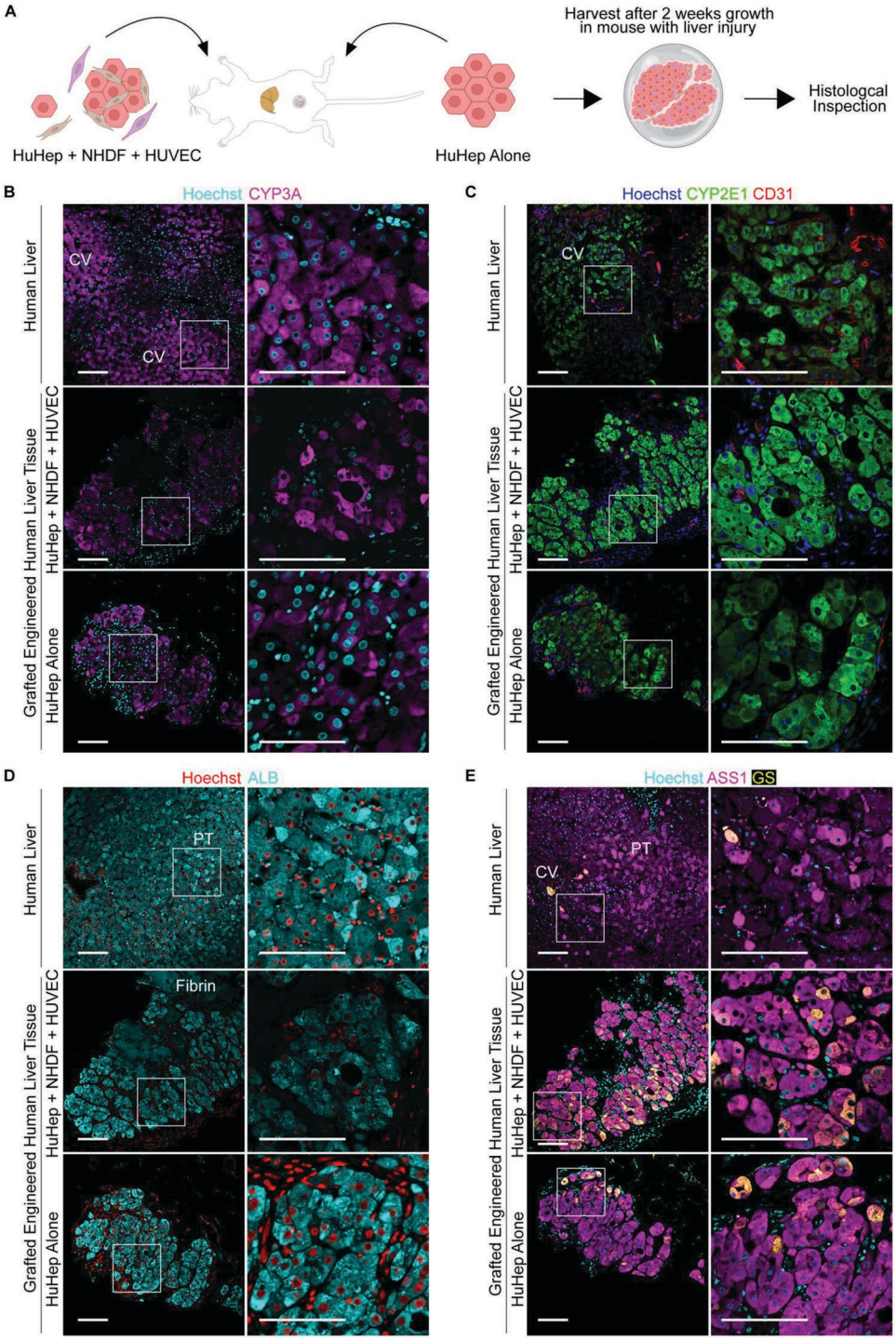

Figure 4. Human NPC are not required for the zonated phenotype in engineered liver tissue. A) Diagram of experiment design: Grafts were generated from HuHep aggregates with and without NPCs NHDF and HUVEC. After two weeks of growth in hosts with liver injury, grafts were collected and stained for histological inspection. B) Immunostaining for cytochrome p450 family 3 subfamily A (CYP3A, pink) and DNA (Hoechst, cyan) in human liver tissue (top), and engineered liver tissue grafts generated with NPC (middle) and without NPC (bottom) and grown in vivo for 2 weeks. C) Immunostaining for CYP2E1 (green), endothelial marker cluster of differentiation 31 (CD31, red), and DNA (Hoechst, blue) in human liver tissue (top), and engineered liver tissue grafts generated with NPC (middle) and without NPC (bottom) and grown in vivo for 2 weeks. D) Immunostaining for ALB (cyan) and DNA (Hoechst, red) in human liver tissue (top), and engineered liver tissue grafts generated with NPC (middle) and without NPC (bottom) and grown in vivo for 2 weeks. E) Immunostaining for ASS1 (pink), GS (yellow), and DNA (Hoechst, blue) in human liver tissue (top), and engineered liver tissue grafts generated with NPC (middle) and without NPC (bottom) and grown in vivo for 2 weeks. In Figure 4B–E, scale bars display 100 µm. CV = central vein, PT = portal triad. ≥3 grafts from separate mouse hosts were stained for each panel; one representative graft is shown.

Factors that regulate liver zonation include the availability of oxygen across the lobule and the Wnt pathway.[7,23–26] In rodents, Wnt ligands from liver central vein endothelial cells regulate β-catenin and induce GS expression.[24,25] Based on this, we initially hypothesized that the HUVEC NPC within the engineered liver tissues would not only support hepatocyte growth, as has been previously shown,[9] but also support a zonation phenotype. Surprisingly, the engineered livers showed a zonated phenotype in the absence of human NPC from graft formulation. Wnt proteins are not traditionally described as circulating to distant sites or acting as hormones, making it unlikely that Wnts derived from the host liver would affect the ectopic graft. The observation that GS was largely expressed adjacent to host tissue suggests that endothelial cells from the host fat pad may be a source of Wnts and promote a zonated phenotype in the graft. Alternatively, this conundrum may support the notion that circulatory factors, such as nutrients or high ammonia levels, are partly responsible for the expression of zonated proteins such as GS, ASS1, ARG1, and HAL. In this case, Wnt signaling may thus be a lesser contributor to the re-establishment of zonation in engineered human liver tissue generated from *adult* hepatocytes. The mechanisms for Wnt transport and contribution to zonation in the human setting, at least in engrafted human liver tissues, are yet to be unveiled.

Intensive engineered devices that establish gradients of nutrients or oxygen exposure are necessary to study human zonation in vitro.[34–46] To our knowledge, this is the first report of an engineered human-derived zonated phenotype in vivo. Future studies could leverage this system to uncover mechanisms of both human hepatocyte expansion and zonation in vivo or to create zonated human liver tissues for the treatment of liver disease.

4. Experimental Section

All procedures involving animals were reviewed and approved by the Institutional Animal Care and Use Committee (IACUC) of the University of Washington under IACUC protocol number: 4388-01.

Cell Sources: All human cells were de-identified and sourced from a vendor. Cryopreserved primary human hepatocytes were purchased from Thermo Fisher Scientific, lot hu1880 (34-year-old, white, female donor) was used in Figures 1 and 3, lot hu8375 (19-year-old, white, female donor) was used for Figure 4. HUVEC and NHDF were purchased from Lonza and used at passage <8. HUVEC were maintained in dishes in endothelial growth media-2 (Lonza), and NHDF were maintained in Dulbecco's modified Eagle medium (DMEM, Thermofisher Scientific) with 10% fetal bovine serum (FBS, Gibco) and 1% penicillin-streptomycin (pen strep, VWR).

Aggregate Culture: Aggregates were generated as previously described.[5,43] Briefly, human primary hepatocytes were thawed and immediately plated into pluronic-coated AggreWell micromolds at 600,000 cells per well on a 6-well plate. Aggregates of HuHep with NHDF were generated by adding 1 million NHDF cells per well at the time of plating. Cells were incubated overnight to gravity-settle and form aggregates in high glucose DMEM with 10% FBS; 1% insulin, transferrin, sodium selenite supplement (BD Biosciences); 0.49 pg mL^{-1} glucagon; 0.08 ng mL^{-1} dexamethasone; 0.018 M hydroxyethyl piperazineethanesulfonic acid; and 1% pen strep.

Graft Construction: To create hepatic aggregates, HuHep were thawed and immediately plated into AggreWell micromolds along with NHDF (≈100 HuHep and 160 NHDF per aggregate) and incubated overnight.[47] HUVEC and hepatic aggregates were then suspended into 10 mg ml^{-1} fibrin at a concentration of 1,250,000 HUVEC mL^{-1} and 45 000 aggregates mL^{-1} and allowed to polymerize within a 16 mm diameter polydimethylsulfoxide circular mold. Engineered tissues were cut with a 6 mm biopsy punch immediately before implantation. Each engineered tissue contained ≈450,000 HuHep, 720,000 NHDF, and 125,000 HUVEC upon implantation.

Graft Implantation: All experiments were performed in female FRGN mice, an immune-deficient model of hereditary tyrosinemia type I. This model was chosen because previous studies by our group and others have shown that regenerative stimuli from liver injury were necessary for hepatic graft expansion and rearrangement after implant. That is, without liver injury, engineered tissues exhibit diminished graft growth and did not self-assemble to resemble native liver.[9,10,47] For all studies here, FRGN mice were anesthetized using isoflurane, and bioartificial tissues were implanted onto the perigonadal fat pads. Three 6 mm tissues per mouse were ligated to the fat by passing a 5-0 suture through both the construct and the fat. Surgical incisions were closed aseptically, and mice were administered 1 mg kg^{-1} buprenorphine (slow releasing). NTBC was withdrawn from animals' drinking water immediately after implantation.

Mouse Model of Liver Injury: The FRGN mouse strain is an immune-deficient model of hereditary tyrosinemia type I, an established model of chronic liver injury. These mice experience progressive liver failure unless the small molecule NTBC is administered in the animals' drinking water. Upon artificial tissue implantation, NTBC was cycled on/off to induce moderate liver injury using established protocols.[8]

Number of Animals Studied: Power calculations in which one tissue was implanted into a given mouse assume an alpha (*p*-value) of 0.05 and a power of 0.90. Based on our previous studies, a sample size of 8 was adequate to detect statistically significant differences in liver injury studies. To allow for mortality in liver injury studies in which animals were cycled on/off NTBC (typically 20% mortality), an additional two animals were enrolled per group to bring the total to 10 animals per group per experiment. The number of animals per endpoint at the experiment set up was shown in Figure S1, Supporting Information.

RNA Sequencing: Tissues were excised from animals and placed in RNALater (Thermo Fisher) to stabilize RNA. Tissues were manually dissected to remove excess mouse fat from around the implanted tissue and prevent the overrepresentation of murine transcripts from the downstream sequencing libraries. A standard phenol-chloroform extraction protocol was used to isolate RNA from tissues. RNA concentration was measured through NanoDrop and frozen. Frozen RNA was sent to BGI Genomics (Cambridge, Massachusetts, USA) for sequencing. For RNAseq analysis, reads were aligned to a human reference genome and the number of reads mapped to individual genes and transcripts was counted. Heatmaps to visualize gene expression from RNAseq analysis were generated from the normalized transcripts per million for each gene using R and RStudio gplots and pheatmap packages. Hierarchical clustering was performed by Pearson correlation on rows and by Spearman for columns; Z-scores were reported.

Gene Set Enrichment Analysis: The significantly impacted pathways and biological processes were analyzed using iPathwayGuide (Advaita Bioinformatics).[48,49] Lists of differentially expressed genes (DEGs) produced during RNAseq analysis were input into the meta-analysis program. Only the following comparisons produced enough DEGs for analysis: week 2 versus week 1, week 4.5 versus week 1, week 7 versus week 1, week 9.5 versus week 1, and week 7 versus week 2.

ELISA: Throughout the experiment and at the time of sacrifice, mice were bled through the saphenous vein, and blood was centrifuged to isolate the serum. Human ALB protein was quantified within mouse serum by ELISA using goat polyclonal capture and horseradish peroxidase (HRP)-conjugated goat anti-human ALB antibodies (Bethyl E80129). Plots were generated using GraphPad Prism.

Immunostaining: Engineered tissues and host auxiliary tissues were harvested and formalin-fixed, paraffin-embedded for histology. Embedded samples were sectioned, and heat-induced antigen retrieval was performed in a pressure cooker with sodium citrate buffer. Samples were blocked with 1.5% normal goat serum, followed by

Table 1. List of antibodies used for immunostaining.

Antibody target	Supplier	Catalog	Host species	Dilution
CK18	Agilent	M701029-2	Mouse	1:100
CK19	Abcam	ab52625	Rabbit	1:250
ALB	Bethyl	A80-129A	Goat	1:100
Vimentin	Abcam	ab45939	Rabbit	1:1000
CD31	Agilent	M0823	Mouse	1:20
ARG1	Sigma	HPA003595	Rabbit	1:400
CYP2A6	Sigma	HPA047262	Rabbit	1:200
ASS1	Sigma	HPA020934	Rabbit	1:200
HAL	Sigma	HPA038547	Rabbit	1:200
GS	Millipore	MAB302	Mouse	1:100
CYP2E1	Abcam	ab28146	Rabbit	1:100
Hu Mitochondria	Abcam	ab92824	Mouse	1:800
ECAD	R&D	AF748	Mouse	1:100
BCAT	Cell signaling	mAb #8480	Rabbit	1:100
CYP3A	Santa Cruz	sc-365415	Mouse	1:100

incubation with primary antibodies listed in **Table 1** overnight at 4 °C, and incubation with secondary antibodies for 1 h at room temperature or overnight at 4 °C. Secondary antibodies used were donkey anti-goat Alexa Fluor 488 (Invitrogen), donkey anti-goat IgG Alexa Fluor 488 conjugate (Invitrogen), donkey anti-mouse Alexa Fluor 555 conjugate (Invitrogen), donkey anti-rabbit immunoglobulin G (IgG) Alexa Fluor 594 conjugate (Novex), and goat anti-mouse IgG1 Alexa Fluor 555 conjugate (Novex). Nuclei were counterstained with Hoechst or DAPI. Immunohistochemical detection of human mitochondria was performed using a mouse-specific HRP/3,3′-diaminobenzidine avidin-biotin complex Detection immunohistochemistry kit (Abcam ab64259). Images were acquired using the microscopes specified in the following section.

Microscopy: Images were acquired using a Nikon wide-field epifluorescence microscope, Nikon A1R confocal, and Yokogawa W1 spinning disk confocal. All microscopes were run using Nikon Elements software. The widefield microscope was an inverted Nikon Eclipse TiE system with a 120BOOST LED-based illumination system and equipped with a Photometrics HQ2 CoolSnap camera and motorized XY stage. The Nikon A1R point scanning confocal system was run on an inverted Nikon Eclipse TiE base with 405-, 488-, 568- and 647 nm excitation laser lines and four detectors: two GaAsP and two Alkali PMTs with a motorized XY stage. The Yokogawa W1 spinning disk confocal has an inverted Nikon Eclipse TiE base and 100 mW 405-, 490-, 561-, and 640 nm lasers, equipped with an Andor iXon 888 Life EMCCD camera linked with a 10-position filter wheel and a motorized XY stage. The spinning disk system was enclosed in an environmental chamber with temperature and local carbon dioxide concentration control.

EdU Staining and Quantification: Animals were injected with 50 mg/kg EdU (Thermo Fisher) 1 h before sacrifice. At the time of sacrifice, animal tissues (peritoneal implants and fat pads, liver, and small intestine) were excised, rinsed in phosphate-buffered saline, and fixed in 4% paraformaldehyde at 4 °C for 2 days. After fixation, tissues were dehydrated to 70% ethanol, paraffin-embedded, and sectioned into 6 mm-thick sections for mounting onto histology slides. To visualize EdU incorporation in HuHep undergoing DNA replication at the time of injection, slides were deparaffinized and co-stained with an Alexa Fluor 647 click chemistry conjugation kit (Invitrogen Click-iT), mouse anti-human CK18, and Hoechst. Images were acquired using a wide-field epifluorescence microscope (listed above). To quantify percent positive hepatocyte nuclei, ilastik software (ilastik.org) was trained to recognize EdU-positive Hoechst-positive nuclei within CK18-positive cells. This training was performed on three images from different animal groups to ensure training diversity. ilastik's Density Count feature was used to count the EdU-positive hepatocyte nuclei, and all images were batch processed to ensure they were counted identically. The total nucleus count was performed using the same process, but by training the software to recognize all Hoechst-positive nuclei within CK18-positive cells, not just the EdU-positive nuclei. The EdU-positive number was divided by the total nucleus count to obtain a percentage of total nuclei undergoing DNA replication at the time of EdU incorporation.

Statistical Analysis: Details regarding preprocessing of data, data presentation (e.g., mean +/- standard deviation), sample size (n for statistical analysis), which statistical methods were used to assess significant differences (name of statistical tests, testing level, adjustments), and software were included in the applicable sections above. GraphPad Prism was used to plot data and perform statistical analyses.

We acknowledge that papers authored by women and scholars from historically excluded racial and ethnic groups are systematically undercited. So that the authors are not further perpetuating this problem, we have made every attempt to reference relevant papers in a manner that is equitable in terms of gender and racial representation.

Supporting Information

Supporting Information is available from the Wiley Online Library or from the author.

Acknowledgements

C.L.F. and T.N.M. contributed equally to this work. This research was funded by NIH NIDDK R01DK128551 (K.R.S.), the NCATS Translational Research Training Program TL1 TR002318 and the NIGMS Molecular Medicine Training Grant T32 GM095421 (C.L.F), the Environmental Pathology/Toxicology NIEHS training program T32 ES007032 and the NSF Postdoctoral Fellowship in Biology Award Number 2109919 (T.N.M.), NIH NIBIB Cardiovascular training grant T32 EB001650 (S.H.S.), and the University of Washington (UW) Post-Baccalaureate Research Education Program (C.B.A.). Any opinions, findings, conclusions, or recommendations expressed in this material are those of the author(s) and do not necessarily reflect the views of the funders. Figures were created with BioRender.com. The authors thank Dr. Dale Hailey from the UW Garvey Imaging Core for assistance with imaging. The authors thank Dr. Theo Bammler and Dr. Lu Wang of the Integrative Environmental Health Sciences Facility Core as part of the Interdisciplinary Center for Exposures, Diseases, Genomics, and Environment at UW. The authors thank all the fantastic animal husbandry and veterinary staff in the UW Department of Comparative Medicine's vivarium. The authors thank all patient tissue donors for their generous contributions to science. The authors acknowledge that the experiments described in this text were conducted on the land of the past, present, and future Coast Salish peoples, the land that touches the shared waters of all tribes and bands within the Suquamish, Tulalip, and Muckleshoot nations; the authors honor the land itself and these Coast Salish tribes.

Conflict of Interest

The authors declare no conflict of interest.

Data Availability Statement

The data that support the findings of this study are available from the corresponding author upon reasonable request.

Keywords

bioengineering, liver, metabolism, RNAseq, zonation

Received: July 21, 2022
Revised: September 23, 2022
Published online:

[1] S. Cheemerla, M. Balakrishnan, *Clin. Liver. Dis.* **2021**, *17*, 365.
[2] S. Wang, M. Toy, T. T. Hang Pham, S. So, *PLoS One* **2020**, *15*, e0239393.
[3] R. Rosenblatt, N. Wahid, K. J. Halazun, A. Kaplan, A. Jesudian, C. Lucero, J. Lee, L. Dove, A. Fox, E. Verna, B. Samstein, B. E. Fortune, R. S. Brown, *Hepatology* **2021**, *74*, 1523.
[4] A. Ward, D. K. Klassen, K. M. Franz, S. Giwa, J. K. Lewis, *Curr. Opin. Organ Transplant.* **2018**, *23*, 336.
[5] S. N. Bhatia, G. H. Underhill, K. S. Zaret, I. J. Fox, *Sci. Transl. Med.* **2014**, *6*, 245sr2.
[6] E. Trefts, M. Gannon, D. H. Wasserman, *Curr. Biol.* **2017**, *27*, R1147.
[7] T. Kietzmann, *Redox Biol.* **2017**, *11*, 622.
[8] S. H. Saxton, K. R. Stevens, *J. Hepatol.* **2022**, https://www.journal-of-hepatology.eu/article/S0168-8278(22)02920-8/fulltext.
[9] K. R. Stevens, M. A. Scull, V. Ramanan, C. L. Fortin, R. R. Chaturvedi, K. A. Knouse, J. W. Xiao, C. Fung, T. Mirabella, A. X. Chen, M. G. Mccue, M. T. Yang, H. E. Fleming, K. Chung, Y. P. De Jong, C. S. Chen, C. M. Rice, S. N. Bhatia, *Sci. Transl. Med.* **2017**, *9*, eaah5505.
[10] A. Vogel, I. E. T. Van Den Berg, M. Al-Dhalimy, J. Groopman, C.-N. Ou, O. Ryabinina, M. S. Iordanov, M. Finegold, M. Grompe, *Hepatology* **2004**, *39*, 433.
[11] R. J. Schulze, M. B. Schott, C. A. Casey, P. L. Tuma, M. A. Mcniven, *J. Cell Biol.* **2019**, *218*, 2096.
[12] I. V. Kholodenko, K. N. Yarygin, *Biomed Res. Int.* **2017**, *2017*, 8910821.
[13] T. Suzuki, Y. Kanai, T. Hara, J. Sasaki, T. Sasaki, M. Kohara, T. Maehama, C. Taya, H. Shitara, H. Yonekawa, M. A. Frohman, T. Yokozeki, Y. Kanaho, *Mol. Cell. Biol.* **2006**, *26*, 6149.
[14] R. Zhao, A. J. Watt, J. Li, J. Luebke-Wheeler, E. E. Morrisey, S. A. Duncan, *Mol. Cell. Biol.* **2005**, *25*, 2622.
[15] B. Morio, B. Panthu, A. Bassot, J. Rieusset, *Cell Calcium* **2021**, *94*, 102336.
[16] A. Husson, C. Brasse-Lagnel, A. Fairand, S. Renouf, A. Lavoinne, *Eur. J. Biochem.* **2003**, *270*, 1887.
[17] R. W. Caldwell, P. C. Rodriguez, H. A. Toque, S. P. Narayanan, R. B. Caldwell, *Physiol. Rev.* **2018**, *98*, 641.
[18] E. M. Mcdonagh, C. Wassenaar, S. P. David, R. F. Tyndale, R. B. Altman, M. Whirl-Carrillo, T. E. Klein, *Pharmacogenet. Genomics* **2012**, *22*, 695.
[19] H. Hammer, F. Schmidt, P. Marx-Stoelting, O. Pötz, A. Braeuning, *Arch. Toxicol.* **2021**, *95*, 117.
[20] T. Omura, *Chem. Biol. Interact.* **2006**, *163*, 86.
[21] A. I. Su, M. P. Cooke, K. A. Ching, Y. Hakak, J. R. Walker, T. Wiltshire, A. P. Orth, R. G. Vega, L. M. Sapinoso, A. Moqrich, A. Patapoutian, G. M. Hampton, P. G. Schultz, J. B. Hogenesch, *Proc. Natl. Acad. Sci. USA* **2002**, *99*, 4465.
[22] L.-L. Hsiao, F. Dangond, T. Yoshida, R. Hong, R. V. Jensen, J. Misra, W. Dillon, K. F. Lee, K. E. Clark, P. Haverty, Z. Weng, G. L. Mutter, M. P. Frosch, M. E. Macdonald, E. L. Milford, C. P. Crum, R. Bueno, R. E. Pratt, M. Mahadevappa, J. A. Warrington, G. Stephanopoulos, G. Stephanopoulos, S. R. Gullans, *Physiol. Genomics* **2001**, *7*, 97.
[23] Z. D. Burke, K. R. Reed, S. W. Yeh, V. Meniel, O. J. Sansom, A. R. Clarke, D. Tosh, *Sci. Rep.* **2018**, *8*, 2735.
[24] Z. D. Burke, K. R. Reed, T. J. Phesse, O. J. Sansom, A. R. Clarke, D. Tosh, *Gastroenterology* **2009**, *136*, 2316.
[25] J. Yang, L. E. Mowry, K. N. Nejak-Bowen, H. Okabe, C. R. Diegel, R. A. Lang, B. O. Williams, S. P. Monga, *Hepatology* **2014**, *60*, 964.
[26] S. Mehta, S. Hingole, V. Chaudhary, *Front. Cell. Dev. Biol.* **2021**, *9*, 714746.
[27] M. Uhlén, L. Fagerberg, B. M. Hallström, C. Lindskog, P. Oksvold, A. Mardinoglu, Å. Sivertsson, C. Kampf, E. Sjöstedt, A. Asplund, I. Olsson, K. Edlund, E. Lundberg, S. Navani, C. A. l.-K. Szigyarto, J. Odeberg, D. Djureinovic, J. O. Takanen, S. Hober, T. Alm, P.-H. Edqvist, H. Berling, H. Tegel, J. Mulder, J. Rockberg, P. Nilsson, J. M. Schwenk, M. Hamsten, K. Von Feilitzen, M. Forsberg, et al, *Science.* **2015**, *347*, 1260419.
[28] R. Ma, A. S. Martínez-Ramírez, T. L. Borders, F. Gao, B. Sosa-Pineda, *Elife* **2020**, *9*, e46206.
[29] M. J. Caldez, N. Van Hul, H. W. L. Koh, X. Q. Teo, J. J. Fan, P. Y. Tan, M. R. Dewhurst, P. G. Too, S. Z. A. Talib, B. E. Chiang, W. Stünkel, H. Yu, P. Lee, T. Fuhrer, H. Choi, M. Björklund, P. Kaldis, *Dev. Cell* **2018**, *47*, 425.
[30] J. Huang, D. A. Rudnick, *Am. J. Pathol.* **2014**, *184*, 309.
[31] N. Dragin, M. Smani, S. Arnaud-Dabernat, C. Dubost, I. Moranvillier, P. Costet, J.-Y. Daniel, E. Peuchant, *FEBS Lett.* **2006**, *580*, 3845.
[32] I. J. Marie, C. Dalet, J.-M. Blanchard, C. Astre, A. Szawlowski, B. S. Aubert, H. Joyeux, P. Maurel, *Biochem. Pharmacol.* **1988**, *37*, 3515.
[33] C. Trautwein, T. Rakemann, P. Obermayer-Straub, M. Niehof, M. P. Manns, *J. Hepatol.* **1997**, *26*, 48.
[34] C. Fujino, S. Sanoh, C. Tateno, S. Ohta, Y. Kotake, *Toxicol. Appl. Pharmacol.* **2019**, *370*, 133.
[35] D. Wolfle, K. Jungermann, *Eur. J. Biochem.* **1985**, *151*, 299.
[36] Y. B. Kang, J. Eo, S. Mert, M. L. Yarmush, O. B. Usta, *Sci. Rep.* **2018**, *8*, 8951.
[37] L. Tomlinson, L. Hyndman, J. W. Firman, R. Bentley, J. A. Kyffin, S. D. Webb, S. Mcginty, P. Sharma, *Front. Bioeng. Biotechnol.* **2019**, *7*, 17.
[38] J. F. Görgens, W. H. Van Zyl, J. H. Knoetze, B. Hahn-Hägerdal, *Biotechnol. Bioeng.* **2003**, *73*, 238.
[39] J. W. Allen, *Toxicol. Sci.* **2005**, *84*, 110.
[40] A. W. Tilles, H. Baskaran, P. Roy, M. L. Yarmush, M. Toner, *Biotechnol. Bioeng.* **2001**, *73*, 379.
[41] G. Janani, B. B. Mandal, *ACS Appl. Mater. Interfaces* **2021**, *13*, 24401.
[42] E. Valle-Encinas, M. Dawes, C. Velasco Martinez, K. McSweeney, M. Müller, T. Bird, T. Dale, *bioRxiv* **2021**, 04.01.438073.
[43] F. T. Lee-Montiel, S. M. George, A. H. Gough, A. D. Sharma, J. Wu, R. Debiasio, L. A. Vernetti, D. L. Taylor, *Exp. Biol. Med.* **2017**, *242*, 1617.
[44] X. Li, S. M. George, L. Vernetti, A. H. Gough, D. L. Taylor, *Lab Chip* **2018**, *18*, 2614.
[45] F. Tonon, G. G. Giobbe, A. Zambon, C. Luni, O. Gagliano, A. Floreani, G. Grassi, N. Elvassore, *Sci. Rep.* **2019**, *9*, 13557.
[46] M. Danoy, S. Poulain, M. Lereau-Bernier, S. Kato, B. Scheidecker, T. Kido, A. Miyajima, Y. Sakai, C. Plessy, E. Leclerc, *Biotechnol. Prog.* **2020**, *36*, e3013.
[47] K. R. Stevens, M. D. Ungrin, R. E. Schwartz, S. Ng, B. Carvalho, K. S. Christine, R. R. Chaturvedi, C. Y. Li, P. W. Zandstra, C. S. Chen, S. N. Bhatia, *Nat. Commun.* **2013**, *4*, 1847.
[48] S. Ahsan, S. Drăghici, *Curr. Protoc. Bioinformatics* **2017**, *57*, 7.15.1.
[49] A. L. Tarca, S. Draghici, P. Khatri, S. S. Hassan, P. Mittal, J.-S. Kim, C. J. Kim, J. P. Kusanovic, R. Romero, *Bioinformatics* **2009**, *25*, 75.